



Microstructures and microhardness for sheets and TIG welded joints of TA15 alloy using friction stir spot processing

Xia-wei YANG, Wen-ya LI, Hong-yu LI, Shuo-tian YAO, Yi-xuan SUN, Yi-xian SUN, Lu MEI

State Key Laboratory of Solidification Processing, Shaanxi Key Laboratory of Friction Welding Technologies, Northwestern Polytechnical University, Xi'an 710072, China

Received 5 August 2016; accepted 19 December 2016

Abstract: Effects of friction stir spot processing (FSSP) on the microstructures and microhardness of tungsten inert gas (TIG) welded TA15 titanium alloy joints were investigated. The macro/micro structural observation and microhardness evaluation of the TA15 alloy sheets and TA15 TIG welded joints were carried out using optical microscope and microhardness tests. The results show that FSSP effectively improves the microstructure and increases the microhardness of the TA15 sheets. As for the TIG welded joints, FSSP also effectively improves the microstructure of joints. And the average microhardness value in weld nugget zone is improved significantly, while a small increase of this value in heat affected zone is observed. The hardness in stirring zone is significantly higher than that in the base metal. Two peak values of hardness appear along the width direction in stirring zone. After FSSP, the average hardness of the weld zone of TA15 TIG welded joint is significantly higher than that before FSSP. Under the present process parameters, both the surface oxidation in TA15 sheets and in TIG welded joints after FSSP are not evident, while the surface forms the bright white layer, which is composed of a great multitude of fine grains.

Key words: friction stir spot processing; TA15 titanium alloy; TIG welded joint; microstructure; microhardness

1 Introduction

TA15 (Ti–6Al–2Zr–1Mo–1V), a typical near titanium alloy, is usually utilized to manufacture the structural components of aircraft due to its high specific strength, excellent thermal stability, low growth rate of fatigue crack and strong corrosion resistance [1–3]. With the wide applications of titanium and titanium alloy under heavy load and bad conditions, it has more and more high demanding to the performance requirements of titanium and titanium alloy. The thin-plate welded structure produced by TA15 titanium alloy not only significantly reduces the mass of the structure, but also improves the structural integrity. However, coarse grains occur in the heat-affected zone and the fusion zone of TIG welded TA15 titanium alloy joints due to heat concentration and high temperature, which affects the use of TA15 alloy TIG welded components. In order to achieve an excellent performance of welded components, TA15 alloy TIG welded joints need to be treated. As for

the coarse grains in the microstructure of deformed workpieces, severe plastic deformation techniques are the effective method to reduce the grain size. And the coarse grains tend to be broken during severe plastic deformation process. Therefore, in the past few years, severe plastic deformation techniques, such as equal channel angular pressing and accumulating rolling have been investigated extensively in fine-grained metal preparation [4].

Friction stir welding (FSW) is a new solid-state joining technique invented at the Welding Institute (TWI) (Cambridge, United Kingdom) [5,6]. The FSW has been successfully used to produce joints in aluminum, magnesium, titanium, steel and other alloys [6,7–11]. Friction stir spot welding (FSSW) was also developed based on the basic principle of the FSW [12,13]. The FSSW process consists of three steps: plunging, stirring, and retracting [14–17]. Figure 1 shows illustration of the FSSW process. First, the tool rotates at a high angular speed. Then, the tool is forced into workpiece until the tool shoulder contacts the top

Foundation item: Project (51405389) supported by the National Natural Science Foundation of China; Project (3102015ZY024) supported by the Fundamental Research Funds for the Central Universities, China; Project (2014003) supported by the Shanghai Key Laboratory of Digital Manufacture for Thin-walled Structures, China

Corresponding author: Wen-ya LI; Tel: +86-29-88495226; E-mail: liwy@nwpu.edu.cn; yangxiawei@nwpu.edu.cn
DOI: 10.1016/S1003-6326(18)64638-2

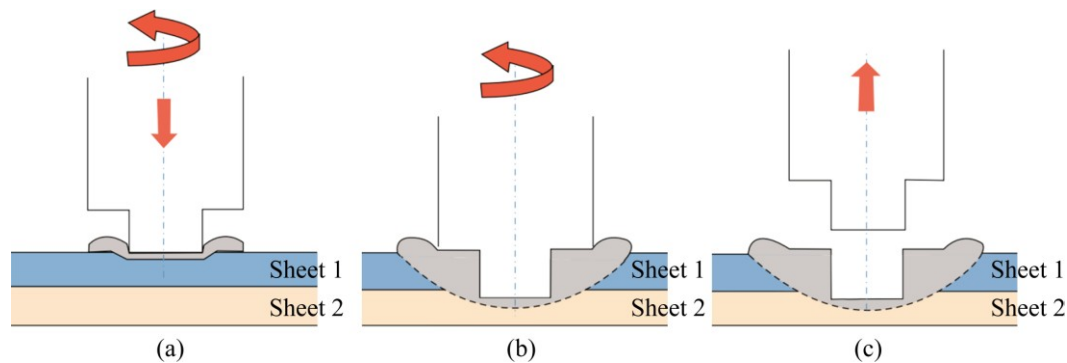


Fig. 1 Illustration of FSSW process: (a) Plunging; (b) Stirring; (c) Retracting [17,18]

surface of the upper workpiece to form a weld spot. The materials are expelled due to the plunging movement of the tool. The stirring stage starts when the tool reaches a predetermined depth and the tool keeps rotating in the workpieces. Frictional heat is generated in the plunging and stirring stages, and thus the materials adjacent to the tool are heated, softened, and mixed in the stirring stage where a solid-state joint will be formed. The tool is retracted from the workpieces when an acceptable bonding is obtained [14–17]. As we know, friction stir processing (FSP) is a novel severe plastic deformation process based on friction stir welding (FSW) [18]. In this work, the friction stir spot processing (FSSP) was selected to study microstructures and microhardness for sheets and TIG welded joints of TA15 alloy. And FSSP is a plastic deformation process based on FSSW.

In the present study, the TA15 alloy sheets were treated first using FSSP, and the macro/micro structural observation and the microhardness evaluation of the FSSP sheets were respectively conducted using optical microscope and microhardness tests. And the macro/micro structural observation and the microhardness evaluation of TA15 TIG welded joints were respectively carried out using FSSP by optical microscope and microhardness tests.

2 Experimental

The investigated material was a 1.5 mm-thick cold-rolled TA15 sheet. Its chemical compositions are (mass fraction): 6.4% Al, 1.3% Mo, 1.8% V, 1.9% Zr, 0.07% O, 0.008% N, 0.005% H and Ti balance. Figure 2 shows microstructure of the as-received TA15 sheet. Figure 3 shows the photo of the as-received TA15 sheet. The dimensions of the original TA15 sheet are 200 mm × 100 mm × 1.5 mm (Fig. 3(a)). The sample of base material for FSSP is shown in Fig. 3(b). And the dimensions of the sample for FSSP are 100 mm × 25 mm × 1.5 mm. As shown in Fig. 4(a), the TA15 TIG

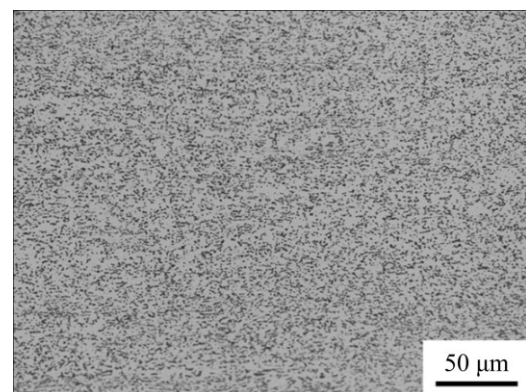


Fig. 2 Microstructure of as-received TA15 sheet

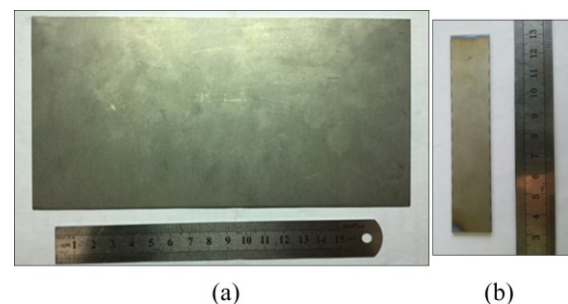
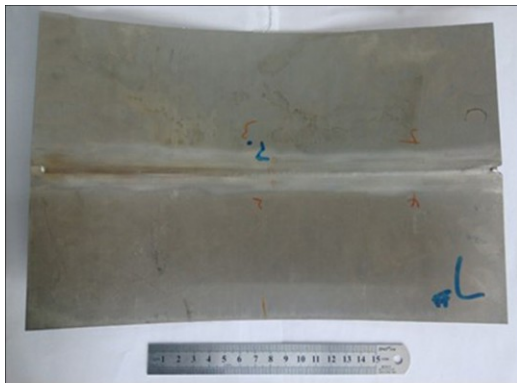


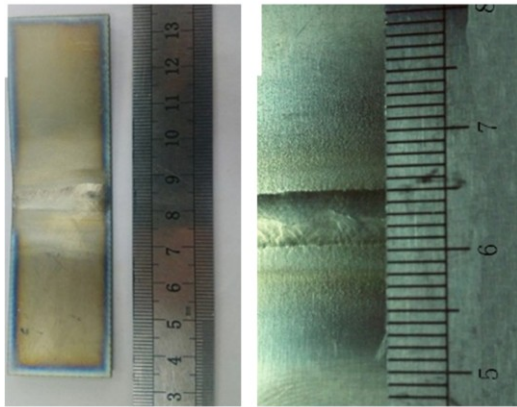
Fig. 3 Photo of as-received TA15 sheet: (a) Original TA15 sheet; (b) Specimen of base material for FSSP

welded sheet was joined by using two sheets of the same size, and dimensions of the sheet are 300 mm × 100 mm × 1.5 mm. Figure 4(b) shows the sample of the welded joints for FSSP and Fig. 4(c) shows the enlarged view for welded joints. And the dimensions of the sample of the welded joints for FSSP are 100 mm × 25 mm × 1.5 mm. Table 1 shows the processing parameters of FSSP. Here, 950 r/min and 1180 r/min were selected as low and high rotating speeds, respectively. A pinless cylindrical tool with the shoulder diameter of 12 mm was used, as shown in Fig. 5, and three involute grooves were machined on the shoulder surface. The tool was made of WC-Co hard alloy.

After FSSP tests, cross-sections of the specimens from TA15 base material sheet and TIG welded joint were subjected to the standard mechanical grinding and polishing routine, and were etched using Kroll solution ($V(\text{HNO}_3):V(\text{HF}):V(\text{H}_2\text{O})=5:10:80$). The optical microscope was observed using Olympus microscope. The microhardness of the specimens was measured by using Struers Duramin-A300 microhardness testing machine. Load and holding time were respectively set as 500 g and 10 s, respectively. Figure 6 shows the schematic diagram of hardness test points. The x -distance between two adjacent points is 500 μm .



(a)



(b)

(c)

Fig. 4 Photos of TA15 TIG welded sheet: (a) Original TA15 TIG welded sheet; (b) Specimen of welded joints for FSSP; (c) Enlarged view for welded joints

Table 1 Processing parameters of FSSP

Sample No.	Pressing speed/ ($\text{mm}\cdot\text{min}^{-1}$)	Reduction/ mm	Rotational speed/($\text{r}\cdot\text{min}^{-1}$)	Stirring time/s
1	30	0.2	950	9
2	30	0.2	950	12
3	30	0.2	950	15
4	30	0.2	1180	9
5	30	0.2	1180	12
6	30	0.2	1180	15

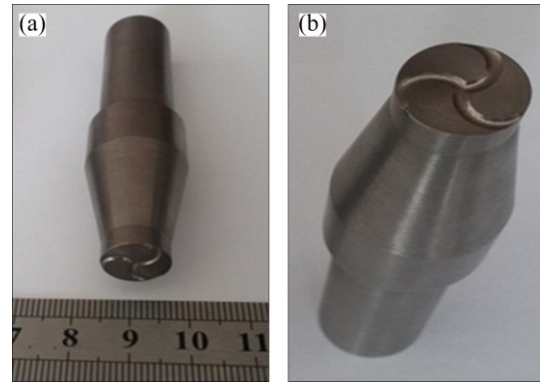


Fig. 5 Photos of FSSP tool: (a) View 1; (b) View 2

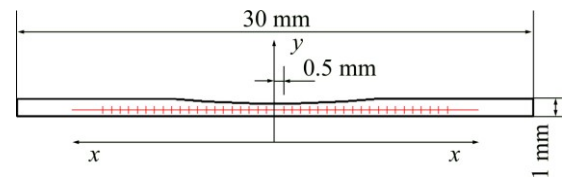


Fig. 6 Schematic diagram of hardness test points

3 Results and discussion

3.1 Macrostructure and microstructure of TA15 sheets after FSSP

Figure 7 shows the macrostructure photo of TA15 specimens after FSSP. Figures 7(a) and (b) respectively show the front side and the reverse side of the FSSP-treated specimens at pressing speed 30 mm/min, reduction 0.2 mm, rotational speed 950 r/min and stirring time of 9, 12 and 15 s. Figures 7(c) and (d) respectively show the front side and the reverse side of the FSSP-treated specimens at pressing speed of 30 mm/min, reduction of 0.2 mm, rotational speed of 1180 r/min and stirring time of 9, 12 and 15 s. It can be seen from Fig. 7 that no evident oxidation occurs on the front surface, while a degree of oxidation occurs on the reverse surface when the experiment was conducted at the rotational speed of 1180 r/min for stirring time 15 s. In addition, the longer the stirring time is, the longer the contact time between the tool and the metal is, so the surface oxidation degree increases with the increase of the stirring time.

Figure 8 shows the cross-section macrostructures of the FSSP-treated TA15 sheet specimens under different stirring time. The pressing speed, the reduction, and the rotational speed are respectively 30 mm/min, 0.2 mm and 950 r/min. The stirring time in Figs. 8(a), (b) and (c) is 9, 12 and 15 s, respectively. And the samples 1, 2, and 3 in Table 1 correspond to Figs. 8(a), (b) and (c), respectively. It can be seen from Fig. 8 that a circular concave shape region appears on the edge of the stirring zone, while the middle part of the stirring zone is

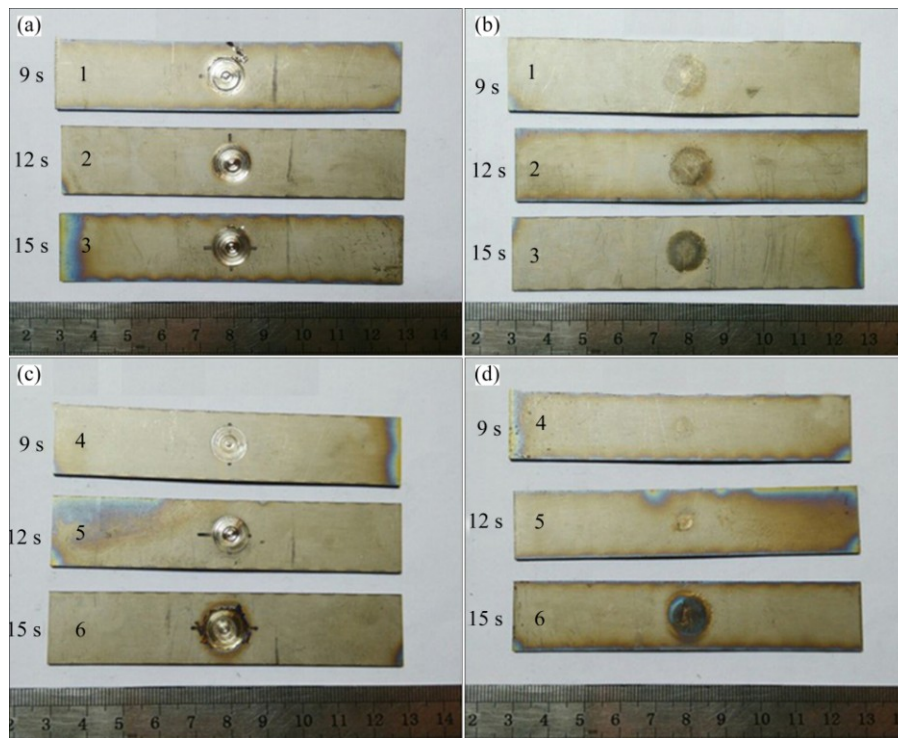


Fig. 7 Macrostructure photos of FSSP-treated TA15 sheet samples at pressing speed 30 mm/min, reduction 0.2 mm, different rotational speeds and different stirring time: (a) Front side of samples at rotational speed 950 r/min; (b) Reverse side of samples at rotational speed 950 r/min; (c) Front side of samples at rotational speed 1180 r/min; (d) Reverse side of samples at rotational speed 1180 r/min

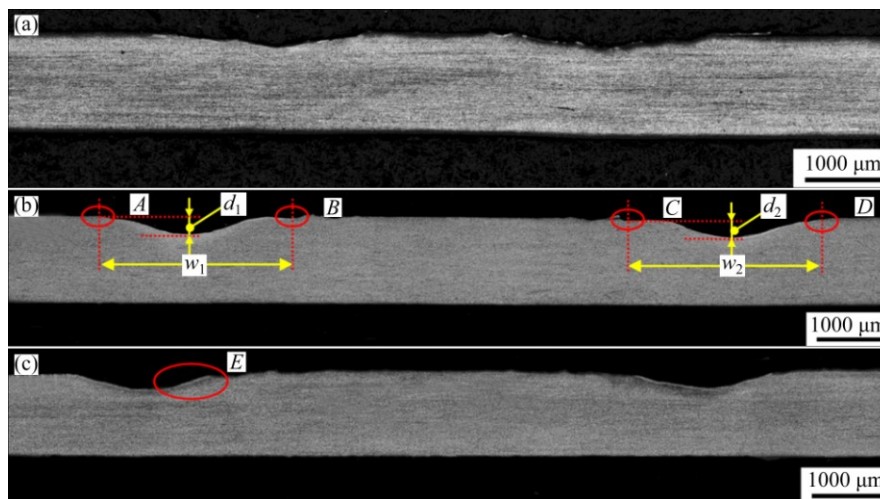


Fig. 8 Cross-section macrostructures of FSSP-treated samples at pressing speed 30 mm/min, reduction 0.2 mm, rotational speed 950 r/min and stirring time 9 s (a), 12 s (b) and 15 s (c)

basically not compressed. The maximum depth of the concave shape region of the FSSP-treated samples in the experiment stirring time of 9 s (Fig. 8(a)) is much less than that in stirring time of 12 s (Fig. 8(b)) and 15 s (Fig. 8(c)). While the maximum depth in stirring time of 12 s (Fig. 8(b)) is almost the same as that in stirring time of 15 s (Fig. 8(c)). In addition, it is found that a bright white layer appears on the surface of the concave shape region. Therefore, in the next paragraph, a detailed explanation/description for the local characteristic

regions of Fig. 8 is given. Here, in order to better illustrate the local characteristic regions, the symbols d_1 , d_2 , w_1 , w_2 , A , B , C and D are given in Fig. 8(b), and the symbol E is given in Fig. 8(c). While the maximum depth in stirring time of 12 s (Fig. 8(b)) is almost the same as that in stirring time of 15 s (Fig. 8(c)), which means that the welding process is in the quasi-steady state.

Figure 9 shows the detail view of the regions A , B , C and D in Fig. 8(b). As shown in Fig. 9, the bright white

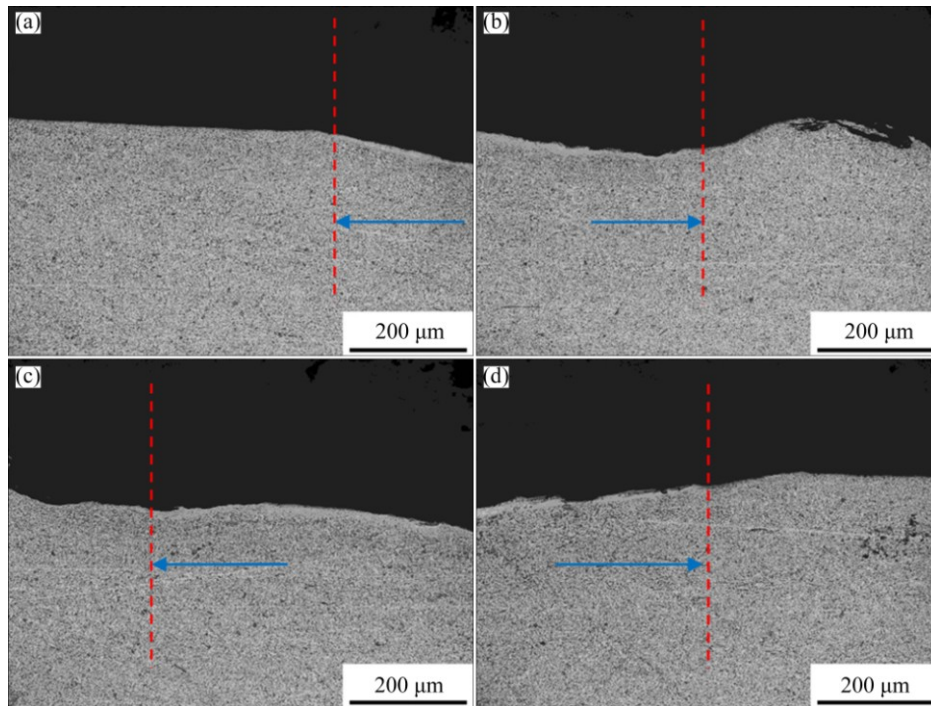


Fig. 9 Microstructures of sample in region *A* (a), region *B* (b), region *C* (c) and region *D* (d) in Fig. 8(b)

layer does not appear on the entire surface of stirring zone, but appears on the local surface. That is, the boundary of the bright white layer can be found. The arrows in Figs. 9(a) and (b) respectively represent the boundary lines of the bright white layer, which respectively correspond to the regions *A* and *B* in Fig. 8(b). The arrows in Figs. 9(c) and (d) respectively represent the boundary lines of the bright white layer, which correspond to the regions *C* and *D* in Fig. 8(b). In addition, the maximum depth of the concave shape zone can be measured according to Fig. 8(b). From Fig. 8(b) and Fig. 9, the values of d_1 , d_2 , w_1 and w_2 can be obtained. And they are 0.25, 0.26, 2.9 and 2.8 mm, respectively.

Figure 10 shows the detail view of the region *E* in Fig. 8(c). As shown in Fig. 10, a clear stratification phenomenon in microstructure is observed. The white layer microstructure was observed evidently in region *F*. The microstructure in region *F* is quite different from that in base material. The transitional region *G* appears between the white layer region *F* and the base material region *H*. In addition, it can be found that region *F* is difficult to corrode during the process of metallographic preparation. The thicknesses of the regions *F* and *G* in Fig. 10 are approximately 60 μm and 95 μm , respectively.

3.2 Macrostructure and microstructure of TA15 TIG welded joints after FSSP treatment

3.2.1 Macrostructure and microstructure of TIG welded joints

Figure 11 shows the macrostructure and micro-

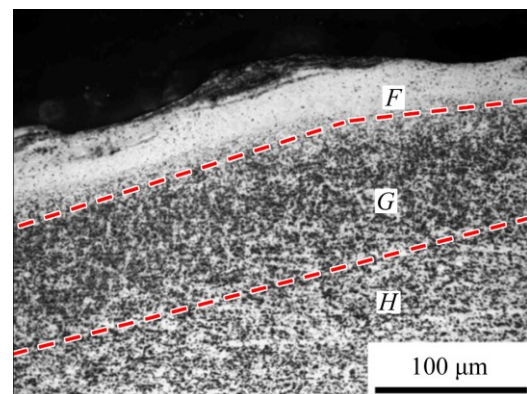


Fig. 10 Microstructure of sample in region *E* in Fig. 8(c)

structure in the cross section of TA15 TIG welded joint. It can be found from Fig. 11(a) that the TA15 sheet deformed during TIG welding process. This is because the nonuniform temperature fields and the nonuniform residual stresses occur during this welding process. In addition, the height in the position of weld seam is larger than other positions. As shown in Fig. 11(a), three zones (weld nugget zone (WNZ), heat affected zone (HAZ) and base material zone (BMZ)) of the joint are observed evidently. The transitional region between HAZ and BMZ can be clearly distinguished (Fig. 11(b)). As shown in Fig. 11(d), the transitional region between WNZ and HAZ can also be clearly distinguished. Widmanstatten structure appears in HAZ (Fig. 11(c)) and in WNZ (Fig. 11(e)). During the TIG welding process, the needle α grains gradually grow and form irregular coarse needle α Widmanstatten structure. The reason is that both a large

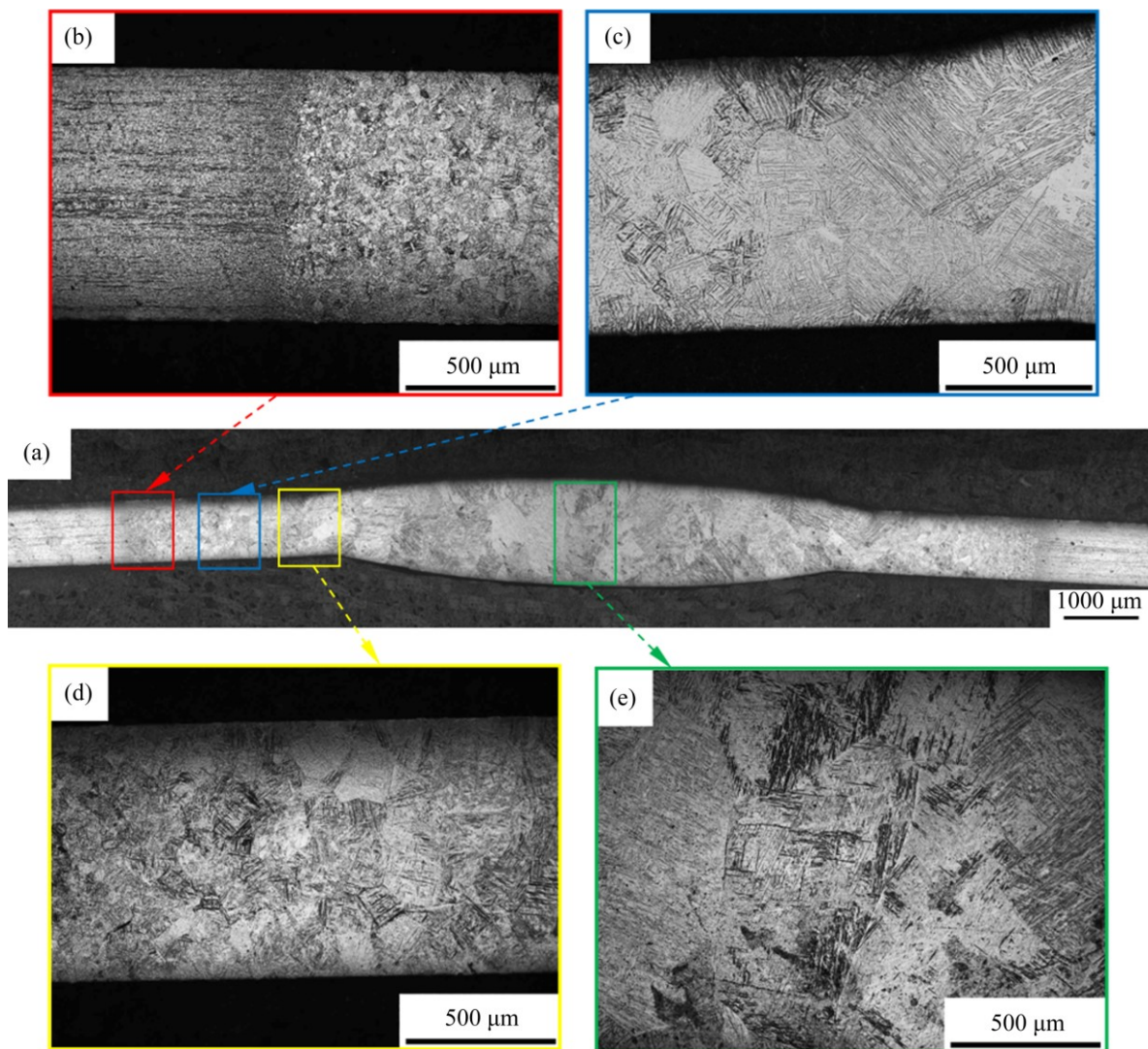


Fig. 11 Macrostructure and microstructure of TIG welded joint in cross section: (a) Macrostructure of joint in cross section; (b) Microstructure of joint in zones between HAZ and BMZ; (c) Microstructure of joint in HAZ; (d) Microstructure of joint in zones between WNZ and HAZ; (e) Microstructure of joint in WNZ

amount of heat and long time heat preservation at high temperature occur during TIG welding process. Meanwhile, it can be found from Fig. 11 that the grain size in HAZ is smaller than that in WNZ. It can be seen from Figs. 11(b) and (d) that microstructure is significantly different in different positions of HAZ. The average grain size of the HAZ near the side of the BMZ is smaller than that near the side of the weld nugget WNZ. In other words, the closer the distance between the selected HAZ position and the WNZ, the greater the average grain size in this selected HAZ position. The amount of heat generated in different positions of HAZ during TIG welding process depends on the distance between the selected HAZ position and WNZ. Effect of heat during TIG welding process on the HAZ that adjacent to the BMZ is relatively small. So, the relatively small grains can be observed in this HAZ (Fig. 11(b)). As shown in Fig. 11(d), the grain size of the HAZ that is

adjacent to the WNZ is larger compared with Figs. 11(b). This is because large impact of heat during welding process on the HAZ is adjacent to the WNZ. As shown in Figs. 11(a) and (e), the WNZ is a typical as-cast microstructure. A large amount of irregular coarse needle α phase (Widmanstatten structure) and a small amount of needle martensite can be observed (Fig. 11(e)). In addition, the maximum grain size reaches approximately 1 mm.

3.2.2 Macrostructure and microstructure of joints after FSSP treatment

Figure 12 shows the macrostructure of TIG welded joint after FSSP treatment. The flash and onion rings were observed in Fig. 12. It can be seen from Fig. 12 that no evident oxidation occurs on the front surface and the reverse surface. Reasons of the formation of the flash and onion rings of TIG welded joint after FSSP treatment are similar to the sheets after FSSP treatment.

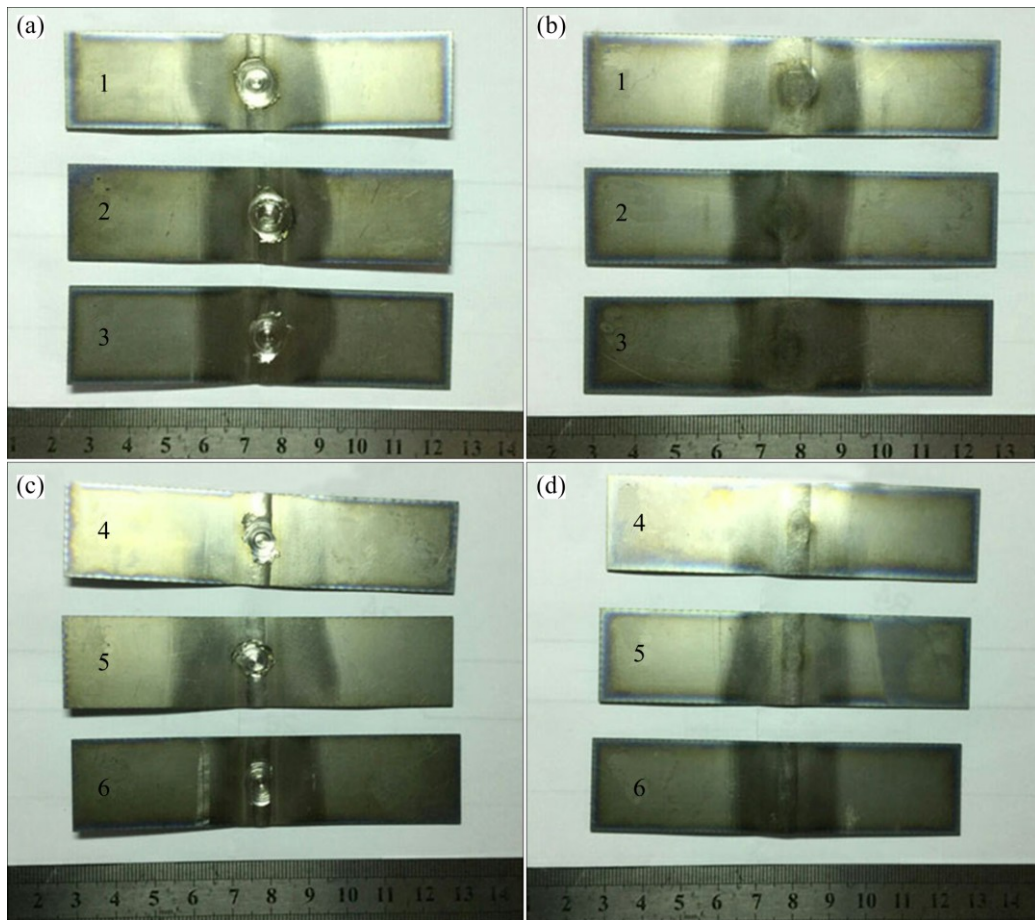


Fig. 12 Macrostructure photos of FSSP-treated TIG welded joint at pressing speed 30 mm/min, reduction 0.2 mm, different rotational speeds and different stirring time: (a) Front side of samples at rotational speed 950 r/min; (b) Reverse side of samples at rotational speed 950 r/min; (c) Front side of samples at rotational speed 1180 r/min; (d) Reverse side of samples at rotational speed 1180 r/min

In addition, under the condition of 1180 r/min, the surface oxidation of sheet in Fig. 7 is much more serious than that of TIG joint in Fig. 12. As for the sheet in Fig. 7, the whole surface is flat. But as for the TIG joint in Fig. 12, there is a bump on the surface of the weld seam of TIG joint. So, the contact surface area between the tool and the sheet surface is larger than that of weld seam surface of TIG joint. Therefore, the surface oxidation of sheet is much more serious than that of TIG joint.

3.2.3 Microstructure of joints after FSSP treatment

Figure 13 shows microstructure of joints after FSSP treatment. As shown in Fig. 13, the characteristic of the microstructure of joints after FSSP treatment can be divided into three types. The upper surface of the sectional microstructure has no evident fluctuation, which is defined as the first type (sample 1, Fig. 13(a)). The upper surface of the sectional microstructure has a significant fluctuation, which is defined as the second type (samples 2, 4 and 6, Figs. 13(b), (d) and (f)). The upper surface of the sectional microstructure has no evident fluctuation but the adhesion of metal appears on the stirring surface, which is defined as the third type (samples 3 and 5, Figs. 13(c) and (e)). As for the

appearance of the adhesion of metal, here are the following explanations. Three involute grooves of stirring tool were adopted in this work and the addition of metal is connected among these three grooves. The material flows in the deformation zone during FSSP due to the mixing action of stirring tool. But when the stirring tool is drawn from the inside of the metal, a small amount of material likely remains at the connection position among these three grooves because the speed of the center position of stirring tool is zero. Therefore, the adhesion of metal possibly appears in sectional microstructure after the next FSSP. In addition, a large amount of heat occurs in the stir zone during FSSP. And a strong interaction force between the stirring tool and the materials in stir zone occurs during FSSP. Therefore, when the stirring tool is drawn from the inside of the metal, a small amount of material likely remains in the involute grooves. And in the next processing process, this material is adhered to the surface of the joint.

Figure 14 shows the microstructures of sample 3 in different positions of heat affect zone (*I*, *J* and *K*, see Fig. 13(c)). As shown in Fig. 14, the cracks occur on the edge of the stir zone between the adhesion of metal and

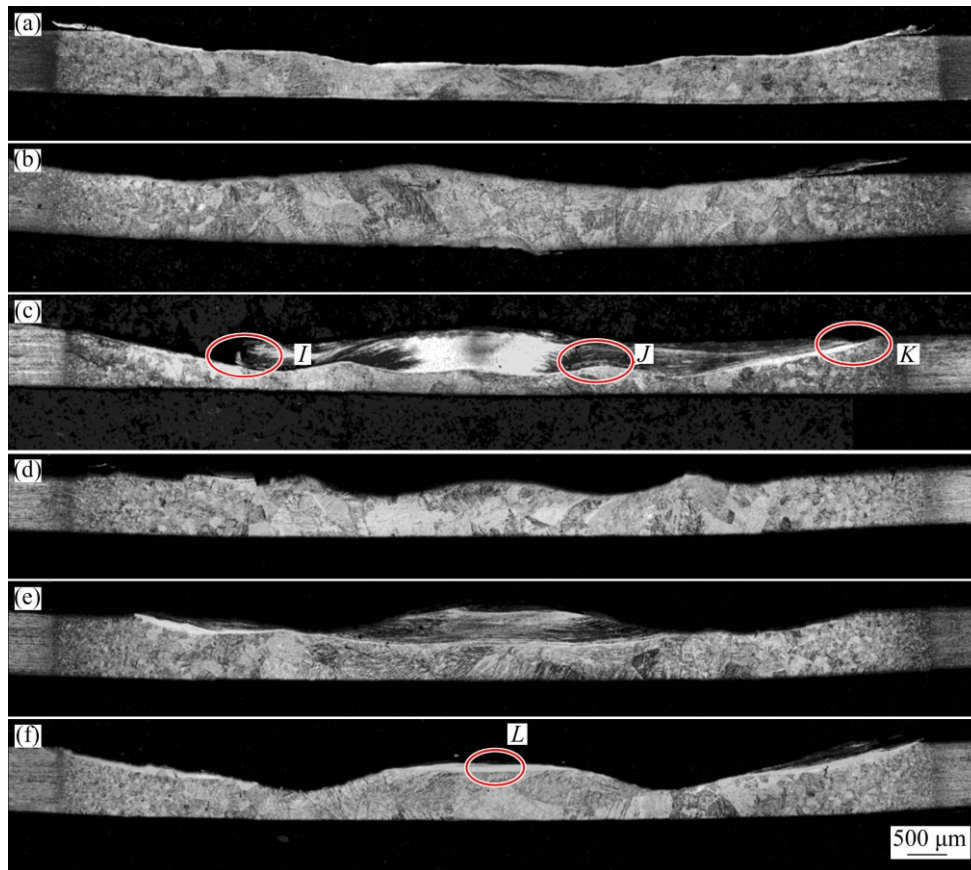


Fig. 13 Microstructures of joints after FSSP treatment under pressing speed 30 mm/min and reduction 0.2 mm: (a) Sample 1, rotational speed 950 r/min, stirring time 9 s; (b) Sample 2, rotational speed 950 r/min, stirring time 12 s; (c) Sample 3, rotational speed 950 r/min, stirring time 15 s; (d) Sample 4, rotational speed 1180 r/min, stirring time 9 s; (e) Sample 5, rotational speed 1180 r/min, stirring time 12 s; (f) Sample 6, rotational speed 1180 r/min, stirring time 15 s

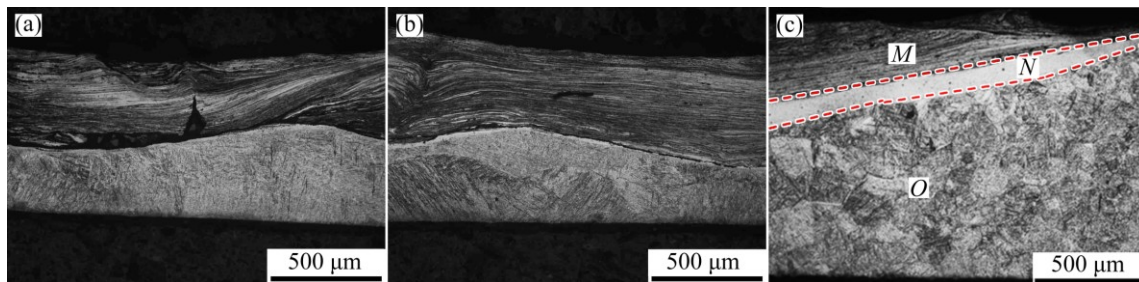


Fig. 14 Microstructures of sample 3 in positions *I* (a), *J* (b) and *K* (c) shown in Fig. 13(c)

the processed sample (Figs. 14(a) and (b)), while in certain areas of the edge, no cracks occur but the bright white layer appears between the adhesion of metal and the FSSP-treated sample (Fig. 14(c)). The materials in stirring zone suffered large tangential force during FSSP, while the materials in the bottom of the TIG sheet suffered small tangential force. Therefore, the materials in stirring zone have a trend of separation, and the cracks formed in stirring zone. In addition, the stratified phenomenon in microstructure was observed in Fig. 14. Figure 15 shows the enlarged view of the microstructure of sample 3 in positions *M* and *N*. The microstructure

with streamline shape can be observed in zone *M* (Fig. 15(a)). The grains in zone *M* were gradually broken and refined due to the drastic stirring action. So, the grains in zone *M* are small. The bright white layer can be observed in zone *N* (Fig. 15(b)). The grains in zone *O* were refined due to the modest stirring action (Fig. 14(c)). The thickness of the region *N* in Fig. 14 is approximately 85 μm .

Figure 16 shows the microstructure of WNZ in sample 6, which corresponds to the zone *L* in Fig. 13(f). The forming mechanism of zones *P* and *Q* in Fig. 16 is similar to that of the zones *M* and *N* in Fig. 14, so it does

not make a detailed description of the forming mechanism of zones *P* and *Q*. The grains in zone *R* were refined due to the drastic stirring action. The thickness of the region *Q* in Fig. 16 is approximately 100 μm .

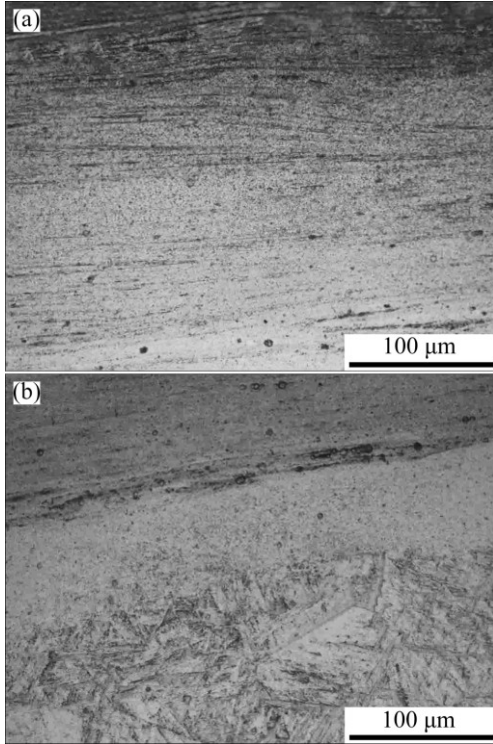


Fig. 15 Microstructures of sample 3 in positions *M* (a) and *N* (b) in Fig. 14(c)

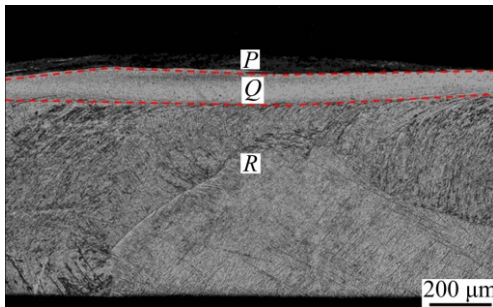


Fig. 16 Microstructure of sample 6 in weld nugget zone

3.3 Microhardness change

Figure 17 shows the microhardness change of the TA15 sheets and TIG welded joint after FSSP treatment with different process parameters. As shown in Fig. 17, the microhardness is present with fluctuating character. It can be seen that the microhardness curve displays symmetrical feature. As shown in Fig. 17(a), the average microhardness values of samples 1, 2 and 3 in stirring zone (-6 mm to 6 mm) are approximately $\text{HV}_{0.5} 351.1$, $\text{HV}_{0.5} 354.6$ and $\text{HV}_{0.5} 355.4$, respectively. While the average microhardness value in base material zone is approximately $\text{HV}_{0.5} 330$. The average hardness of the three groups parameters of FSSP is higher than that of

the base material by 7%. In addition, the peak microhardness appears in two positions (-4 mm and 4 mm), and it is approximately $\text{HV}_{0.5} 379$. As shown in Fig. 8(b) and Fig. 17(a), when the zone is adopted in the bright white layer (-5.4 mm to -2.5 mm and 2.5 mm to 5.4 mm), the average microhardness is approximately $\text{HV}_{0.5} 363$, which is higher than the base material by 10%. While the zone is adopted in the stirring zone (-2.5 mm to 2.5 mm), the average microhardness is approximately $\text{HV}_{0.5} 349$, which is higher than the base material by 5.7%.

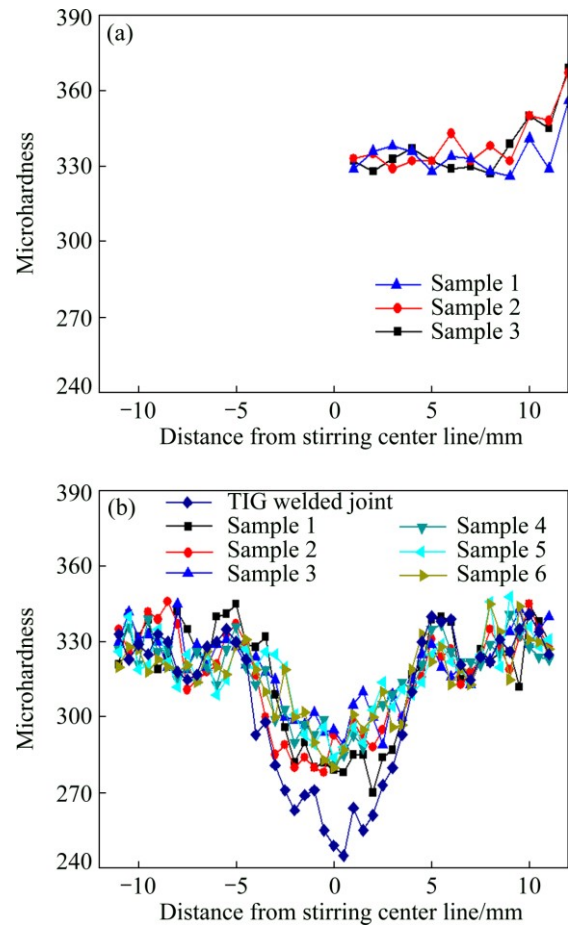


Fig. 17 Microhardness change of TA15 sheets (a) and TIG welded joint (b) after FSSP treatment

As shown in Fig. 17, the microhardness value of base material is evidently higher than that of the TIG welded joint and processed joint. But as shown in Fig. 17(b), the average microhardness value of TIG welded joint after FSSP treatment in stirring zone is evidently higher than that of the TIG welded joint. The average microhardness value of six groups of parameters in weld nugget zone after FSSP treatment is approximately $\text{HV}_{0.5} 294.7$, which is higher than that in the weld nugget zone by 11.5%. While the average microhardness value in heat affected zone after FSSP has no significant increase, which is only higher than that in the heat affected zone by 3.2%.

Because the bright white layer appears in the microstructure of all the test samples. The hardness of bright white layer of TA15 sheets after FSSP treatment was especially given. The average hardness of the bright white layer is approximately $HV_{0.5}$ 363, which is evidently higher than that of the base material.

4 Conclusions

1) As for the TA15 specimens after FSSP treatment, no evident oxidation occurs on the front surface, while a degree of oxidation occurs on the reverse surface when the experiment was conducted at the rotational speed of 1180 r/min and stirring time 15 s. In addition, the surface oxidation degree increases with the increase of the stirring time. A circular concave shape zone appears in the edge of the stirring zone, while the middle zone of the stirring zone is basically not compressed. A bright white layer appears on the surface of the concave shape zone.

2) As for the TIG welded joint, three zones (WNZ, HAZ and BMZ) of the TIG welded joint were observed evidently. A large amount of irregular coarse needle α phase (Widmanstatten structure) and a small amount of needle martensite can be observed in the WNZ.

3) As for the TA15 TIG welded joint after FSSP treatment, the flash and onion rings can be observed from macrostructure photo. The characteristic of the microstructure of joints after FSSP can be divided into three types. The first type is that the upper surface of the sectional microstructure has no evident fluctuation. The second type is that the upper surface of the sectional microstructure has significant fluctuation. The third type is that the upper surface of the sectional microstructure has no evident fluctuation but the adhesion of metal appears on the stirring surface. In addition, the bright white layer in microstructure can be observed in welded joint after FSSP treatment.

4) The average microhardness values of TA15 samples 1, 2 and 3 in stirring zone are approximately $HV_{0.5}$ 351.1, $HV_{0.5}$ 354.6 and $HV_{0.5}$ 355.4, respectively. The average hardness of the three groups of parameters of FSSP is higher than that of the base material by 7%. The average microhardness value of six groups of parameters in WNZ after FSSP treatment is approximately $HV_{0.5}$ 294.7, which is higher than that in the WNZ by 11.5%. While the average microhardness value in HAZ after FSSP treatment is higher than that in the WNZ by 3.2%.

References

[1] DONG X J, LU S Q, ZHENG H Z. Dynamic spheroidization kinetics

- behavior of Ti-6.5Al-2Zr-1Mo-1V alloy with lamellar microstructure [J]. Transactions of Nonferrous Metals Society of China, 2016, 26(5): 1301–1309.
- [2] WU C, YANG H, LI H W. Simulated and experimental investigation on discontinuous dynamic recrystallization of a near- α TA15 titanium alloy during isothermal hot compression in β single-phase field [J]. Transactions of Nonferrous Metals Society of China, 2014, 24(6): 1819–1829.
- [3] HE D, ZHU J C, LAI Z H, LIU Y, YANG X W, NONG Z S. Residual elastic stress-strain field and geometrically necessary dislocation density distribution around nano-indentation in TA15 titanium alloy [J]. Transactions of Nonferrous Metals Society of China, 2013, 23(1): 7–13.
- [4] ZHANG D T, XIONG F, ZHANG W W, QIU C, ZHANG W. Superplasticity of AZ31 magnesium alloy prepared by friction stir processing [J]. Transactions of Nonferrous Metals Society of China, 2011, 21(9): 1911–1916.
- [5] THOMAS W M, NICHOLAS E D, NEEDHAM J C, MURCH M G, TEMPLESMITH P, DAWES C J. Friction Stir Butt Welding: PCT/GB92/02203 [P]. 1991.
- [6] MISHRA R S, MA Z Y. Friction stir welding and processing [J]. Materials Science and Engineering R, 2005, 50(1–2): 1–78.
- [7] NANDAN R, DEBROY T, BHADOSHIA H K D H. Recent advances in friction-stir welding: Process, weldment structure and properties [J]. Progress in Materials Science, 2008, 53(6): 980–1023.
- [8] FONDA R W, KNIPLING K E. Texture development in near- α Ti friction stir welds [J]. Acta Materialia, 2010, 58(19): 6452–6463.
- [9] ZHOU L, LIU H J, LIU P, LIU Q W. The stir zone microstructure and its formation mechanism in Ti-6Al-4V friction stir welds [J]. Scripta Materialia, 2009, 61(6): 596–599.
- [10] WU L H, WANG D, XIAO B L, MA Z Y. Microstructural evolution of the thermomechanically affected zone in a Ti-6Al-4V friction stir welded joint [J]. Scripta Materialia, 2014, 78–79: 17–20.
- [11] ZHANG Y, SATO Y S, KOKAWA H, PARK S H C, HIRANO S. Microstructural characteristics and mechanical properties of Ti-6Al-4V friction stir welds [J]. Materials Science and Engineering A, 2008, 485(1–2): 448–455.
- [12] ZAHRA J S, MOHSEN H S, JALIL V K, CHEN N, SHI Q Y, YAO K F. Microstructure characterization and mechanical properties of Ti-based bulk metallic glass joints prepared with friction stir spot welding process [J]. Materials and Design, 2016, 100: 120–131.
- [13] MUBIAYI M P, AKINLABI E T. Evolving properties of friction stir spot welds between AA1060 and commercially pure copper C11000 [J]. Transactions of Nonferrous Metals Society of China, 2016, 26(7): 1852–1862.
- [14] MERZOUG M, MAZARI M, BERRAHAL L, IMAD A. Parametric studies of the process of friction spot stir welding of aluminium 6060-T5 alloys [J]. Materials and Design, 2010, 31(6): 3023–3028.
- [15] ZHANG Z, YANG X, ZHANG J, ZHOU G, XU X, ZOU R. Effect of welding parameters on microstructure and mechanical properties of friction stir spot welded 5052 aluminum alloy [J]. Materials and Design, 2011, 32 (8–9): 4461–4470.
- [16] NGUYEN N T, KIM D Y, KIM H Y. Assessment of the failure load for an AA6061-T6 friction stir spot welding joint: Proceedings of the Institution of Mechanical Engineers B [J]. Journal of Engineering Manufacture, 2011, 225(10): 1746–1756.
- [17] YANG X W, FU T, LI W Y. Friction stir spot welding: A review on joint macro and microstructure, property, and process modeling [J]. Advances in Materials Science and Engineering. 2014, 2014(1): 1–11.
- [18] MA Z Y. Friction stir processing technology: A review [J]. Metallurgical and Materials Transaction A, 2008, 39: 642–658.

基于搅拌摩擦点加工技术的 TA15 钛合金板及其 TIG 焊接接头组织及硬度

杨夏炜, 李文亚, 李宏宇, 姚硕天, 孙宜璇, 孙怡娴, 梅璐

西北工业大学 凝固技术国家重点实验室 陕西省摩擦焊接工程技术重点实验室, 西安 710072

摘要: 基于搅拌摩擦点焊加工技术(FSSP), 对 TA15 钛合金 TIG 焊接接头的组织和硬度进行研究。采用金相分析和硬度测试方法, 分别对 TA15 板材及其 TIG 焊接接头进行组织分析和硬度测试。结果表明, FSSP 不但能有效改善 TA15 板材组织, 而且可以提高其显微硬度, 同时也可以改善 TA15 合金 TIG 焊接接头的显微组织。焊核区平均显微硬度值显著提高, 热影响区显微硬度值略有增加。搅拌区的硬度明显高于母材, 且沿着宽度方向出现两个硬度峰值。经过 FSSP 之后, TA15 合金 TIG 焊接接头焊核区的平均硬度值与 FSSP 之前相比, 有了显著提高。此外, 在所选工艺参数下, TA15 板材及其 TIG 焊接接头经过 FSSP 之后, 表面氧化均不明显, 同时也发现, 表面均出现晶粒细小的光亮白层组织。

关键词: 搅拌摩擦点加工; TA15 钛合金; TIG 焊接接头; 显微组织; 显微硬度

(Edited by Xiang-qun LI)